ABSTRACT

Title of thesis: TESTING FOR OPTIMAL LARGE-SCALE VEGETATION PROPERTIES FOR MAXIMUM TERRESTRIAL PRODUCTIVITY AND QUANTIFYING FUTURE UNCERTAINTY OF VEGETATION RESPONSE TO ANTICIPATED CLIMATE CHANGE

Ryan Pavlick
Master of Arts, 2007

Thesis directed by: Dr. Axel Kleidon
Max Planck Institute for Biogeochemistry

In this study, I present a new approach to quantifying a range of uncertainty associated with the carbon-climate feedback over the period 1850 to 2100 within an earth system model of intermediate complexity. The degree to which terrestrial vegetation adaptively self-organizes to shape its own climatic conditions is still an open question. Nonetheless, one can simulate a best case scenario, in which terrestrial productivity is periodically maximized with respect to several macroscopic vegetation parameters, commonly held constant in other models such as maximum stomatal conductance. The results of this dynamically optimized simulation are compared to a simulation where the vegetation parameters are held static at the values optimized for pre-industrial conditions. With this comparison, the degree to which terrestrial productivity is underestimated when vegetation parameterizations remain static compared to those reflecting optimal adaptation to new conditions can be quantified.

TESTING FOR OPTIMAL LARGE-SCALE VEGETATION PROPERTIES FOR MAXIMUM TERRESTRIAL PRODUCTIVITY AND QUANTIFYING FUTURE UNCERTAINTY OF VEGETATION RESPONSE TO ANTICIPATED CLIMATE CHANGE

by

Ryan Pavlick

Thesis submitted to the Faculty of the Graduate School of the
University of Maryland, College Park in partial fulfillment
of the requirements for the degree of
Master of Arts
2007

Advisory Committee:
Professor Ralph Dubayah, Chair and Advisor
Dr. Axel Kleidon Co-Advisor
Professor Stephen Prince

Acknowledgments

First and foremost I'd like to thank my advisor, Dr. Axel Kleidon for his support and getting me involved in this line of research. He has always been patient and generous with his time. I look forward to many more years with him as a friend and a colleague.

I would also like to thank Professor Ralph Dubayah and Professor Stephen Prince for serving on my thesis committee and drudging through my manuscript.

I am grateful for the time spent by the IT staff at the Max Planck Institute for Biogeochemistry working out all the little quirks in the computing cluster. Many thanks are due to the Geography administrative staff in for all their help over the years.

I would like to acknowledge financial support from the National Science Foundation (Grant 0513506) and the Max Planck Society.

Table of Contents

List of Figures

List of Abbreviations

α_S	surface albedo (unitless)
c_p	soil heat capacity (J m^{-3} K^{-1})
C_{veg}	vegetation carbon balance (kgC m^{-2})
$C_{veg,above}$	aboveground vegetation carbon (kgCm^{-2})
$C_{veg,below}$	belowground vegetation carbon (kgC m^{-2})
ECMWF	European Center for Medium Range Weather Forecasting
ET	evapotranspiration (mm/day)
ϵ_{lue}	light use efficiency
$f_{veg,above}$	fractional cover of aboveground vegetation (unitless between 0 and 1)
f_{leaf}	fraction of the surface covered by leaves (unitless between 0 and 1)
GPP	gross primary productivity (gC m^{-2} day^{-1})
GPP_{light}	light-limited rate of photosynthesis (gC m^{-2} day^{-1})
GPP_{flux}	flux-limited rate of photosynthesis (gC m^{-2} day^{-1})
gs_{max}	maximum stomatal conductance (unitless)
k	extinction coefficient (unitless)
LAI	leaf area index (m^2/m^2)
LIT	litter fall (gC m^{-2} day^{-1})
P	precipitation (mm/day))
$p\mathrm{CO2}_{,air}$	ambient CO2 concentration (ppm)
$p\mathrm{CO2}_{,leaf}$	internal leaf CO2 concentration (ppm)
P_i	2048x2 array describing the biotic parameters of each grid cell
p_{rs}	fraction of carbon allocated to above-ground biomass (unitless)
Q_{PAR}	photosynthetically active radiation W m^{-2})
Q_{SW}	solar radiation flux at the surface (W m^{-2})
$Q_{SW,net}$	absorbed solar radiation (W m^{-2})
Q_{LW}	terrestrial radiation flux (W m^{-2})
Q_{SH}	surface sensible heat flux (W m^{-2})
Q_{LH}	surface latent heat flux (W m^{-2})
q_{sat}	specific humidity of the surface at saturation (kg/kg)
q_{air}	near-surface air specific humidity (kg/kg)
R	runoff (mm/day)
RES_a	autotrophic respiration (gC m^{-2} day^{-1})
SimBA	SIMulator of Biospheric Aspects
τ_{veg}	mean residence time for vegetation carbon (years)
T_S	near-surface air temperature (K)
W_S	soil water balance (kg/m^2)
$X_{i,n}$	2-vector array describing the biotic parameter values of a land grid cell
$z0_{noveg}$	aerodynamic roughness length of non-vegetated area (m)
$z0_{oro}$	aerodynamic roughness length of the orography (m)
$z0_{srf}$	aerodynamic surface roughness (m)
$z0_{veg}$	aerodynamic roughness length of vegetation (m)

Chapter 1

Introduction

1.1 Climate-Vegetation Interactions

The large-scale patterns of the activity of the terrestrial biosphere are strongly linked to the climatic conditions over land. The availability of light, water, and heat strongly shapes patterns of terrestrial productivity (e.g. Field et al. 1998). These limitations impose constraints on vegetation form and functioning through the land surface energy-, water-, and carbon balances. On the other hand, vegetation plays an important part in shaping the climatic conditions near the land surface. Through its effects on surface albedo, surface roughness, and the depth of the rooting zone, vegetation modulates the exchange fluxes of momentum, energy and mass at the land surface, and thereby affects the overlying atmosphere. The climatic relevance of vegetation has been demonstrated by sensitivity simulations with atmospheric general circulation models (e.g. Shukla and Mintz 1982, Betts 1999, Kleidon et al. 2000). For instance, Kleidon et al. (2000) have shown with a climate model simulation of a Desert World that continental evapotranspiration is substantially reduced in the absence of vegetation, leading to profound changes in the surface energy balance and a substantially weakened hydrologic cycle over land. Such vegetation feedbacks on the physical climatic conditions at the land surface have been shown to play an important role in the present-day climate system (Bonan et al.

1992; Kleidon and Heimann 2000), and its response to global change, for instance in the Mid-Holocene (Foley et al. 1994; Kutzbach et al. 1996; Claussen and Gayler 1997), during ice ages (de Noblet et al. 1996, Kleidon and Lorenz 2001), and in scenarios of anthropogenic future climatic change (Sellers et al. 1996; Betts et al. 1997).

The climate-vegetation system can be described in steady-state by the following set of surface energy and mass balance equations (Bonan 2002). The steady-state surface energy balance can be stated as the balance of the net influx of solar radiation, Q_{SW}, including the effect of surface albedo α_s, the outflux of terrestrial radiation (a function of surface temperature T_S), Q_{LW}, and the sensible and latent heat fluxes, Q_{SH} and Q_{SH}, where c_p is the soil heat capacity.

$$Q_{SW}\,(1\ -\ \alpha_{\mathrm{S}})\ -\ Q_{LW}\,(Ts)\ -\ Q_{SH}\ -\ Q_{LH}\ =\ c_p\,\frac{dTs}{dt}\ =\ 0 \qquad (1.1)$$

The rates of precipitation P, evapotranspiration ET, and runoff R form the expression for the surface water balance, W_S.

$$P\ -\ ET\ -\ R\ =\ \frac{dWs}{dt}\ =\ 0 \qquad (1.2)$$

Finally, a simplified vegetation carbon balance, C_{VEG}, for terrestrial vegetation is given by:

$$GPP\ -\ RES_a\ -\ LIT\ =\ \frac{d\mathrm{C}veg}{dt}\ =\ 0 \qquad (1.3)$$

where GPP is gross primary productivity, RES_a is autotrophic respiration, and LIT is the rate of litter production. The balance equations add to zero when taken as long-term climatological averages.

1.2 Diversity of Vegetation Form and Functioning

One of the unique features of vegetation is that it is inherently diverse and able to adapt to its climatic environment, at the scale of individual plant physiology and through changes in ecosystem composition. This diversity in vegetation form and functioning adds many degrees of freedom to the land surface; allowing the surface energy- and mass fluxes in equations 1.1-1.3 to be partitioned in many different ways. This allows for a wide range of possible values for T_S, W_S, and C_{VEG}. As a consequence, the energy- and mass balances merely act as constraints on what is possible, but are insufficient to determine the full nature of land surface functioning and climate-vegetation interactions. Some examples of macroscopic vegetation properties that moderate the land surface and affect climate functioning include:

- *Maximum stomatal conductance*: Through changes in stomatal behavior and density, vegetation is able to limit rate of transpiration to less than the potential rate (which is ultimately constrained by available water W_S and energy, $Q_{SW,net}$). Increased stomatal conductance increases the supply of atmospheric CO2 for photosynthesis. However, since the uptake of carbon is linked to the transpiration of water, an increase in stomatal conductance on the large-scale will also likely lead to increase in convective cloud cover leading to a decrease in net solar radiation, $Q_{SW,net}$ available for photosynthesis.

- *Root-shoot partitioning*: The allocation of carbon between above-ground and below-ground growth affects the leaf area and the depth of the rooting zone. More carbon allocated to above-ground growth and a higher leaf area will re-

sult in a lower surface albedo, α_S, and more available light for photosynthesis, $Q_{SW,net}$. However, this comes at the cost of less carbon available for roots, decreasing the depth of the rooting zone, limiting the availability of soil moisture for transpiration, ET.

- *Leaf albedo*: Plants have some measure of control over the albedo of their leaf surfaces. In a warmer, water-limited climate, vegetation may adapt leading to an increase the leaf albedo, leading to a higher overall surface albedo, limiting the net solar radiation, $Q_{SW,net}$ and decreasing surface temperatures T_S. Likewise in cooler, light-limited or temperature-limited regions, vegetation may adapt leading to a decrease in leaf albedo, leading to a reduction in surface albedo, more available net solar radiation, and higher surface temperatures.

- *Canopy roughness*: Canopy structure, constrained by the carbon balance and determined by plant forms and ecosystem composition, can affect the aerodynamic roughness of the land surface. A rougher surface generally leads to more efficient turbulent exchange of water and carbon (higher ET), however, it will also likely increase the convective cloud cover (Sud et al. 1988) and therefore decrease net solar radiation, $Q_{SW,net}$.

The immediate question that follows is how vegetation organizes itself in terms of climatologically relevant land surface properties and what the climatic impacts of such adaptive behavior is for the climate of the present-day and for its sensitivity to global change.

One approach that has been used in past studies, mainly at the scale of individual plants, assumes that terrestrial vegetation adapts optimally to its environmental conditions in terms of its form and functioning, thereby maximizing its productivity (gross carbon uptake). Examples of previous work include optimized stomatal functioning (Cowan and Farquhar 1977; Cowan 1977), optimized partitioning of carbon resources within plants between roots and shoots (Thornley 1969, 1972; Dewar 1993), optimized distribution of leaf nitrogen in canopies (Field 1983, Dewar 1996) and several aspects of vegetation with respect to its ecohydrological functioning (Eagleson 2002). One may ask whether the large-scale functioning of terrestrial vegetation is also optimal in terms of its productivity given the constraints of the climatological surface energy- and water balances. This would provide a powerful approach to characterize vegetation functioning in the climate system and how it adapts to change.

1.3 Thesis Outline

The purpose of this study is to examine whether terrestrial vegetation is indeed optimally adapted in terms of its climatic functioning to allow for maximum productivity given present-day conditions and to present a methodology for quantifying the uncertainty in future terrestrial productivity, associated with the degree to which vegetation might adapt at the large, climatically scale relevant adaptation under scenarios of global change. This is an extension of earlier work on optimum rooting depth (Kleidon and Heimann 1998; Kleidon 2004a) and optimum stomatal

functioning (Kleidon 2004b). Several parameters characterizing vegetation form and functioning are varied in a series of sensitivity simulations using an Earth system model of intermediate complexity. The results of the sensitivity analysis are used to determine the range of biologically possible climate-vegetation steady states given the overall energy and water balance constraints. Then, the partitioning of energy fluxes in the optimal climates, those with highest simulated gross primary productivities, is compared with observations from the ECMWF ERA-40 reanalysis climate dataset (Upsalla 2005) at the biome scale. The ratio of turbulent to radiative energy fluxes at the land surface is used as a proxy for the cumulative effect of vegetation form and functioning on overlying atmosphere. This serves as a first crude test to assess whether vegetation productivity, in terms of gross carbon gain, is near its maximum possible value within the climate system, given the constraints of the surface energy and water balance. Under scenarios of global change, vegetation may adapt to a new optimum partitioning of surface fluxes that maintains maximum productivity.

Anthropogenic greenhouse gas emissions are predicted to continue to cause significant changes to the Earth's climate throughout the next century (IPCC 2007). Currently, most of those emissions are taken up by the ocean and the terrestrial biosphere (Prentice et al 2001). The future absorption of carbon by these sinks is sensitive to climatic change (Fung et al 2004). While there are still large uncertainties, most recent modelling studies (e.g. Cox et al 2000, Friedlingstein et al 2001, Zeng et al 2004, Friedlingstein et al 2006) predict that the negative impacts of climate change on the magnitude of the terrestrial carbon sink will cause this carbon-

climate feedback to be positive. A positive carbon-climate feedback means that an external perturbation to the system (the introduction of anthropogenic emissions) lead to climate change, which in turn would lead to changes in the carbon-cycle that amplify the initial external perturbation.

Most of the coupled carbon-climate models used in these previous studies include dynamic vegetation schemes and allow for possible shifts in biomes, however, the parameters that characterize vegetation form and functioning are held static throughout the simulations. This excludes the possibility of macroscopic adaptation of terrestrial vegetation altering the climate through changes in coupling the between land surface and the overlying atmosphere. While the degree to and speed with which terrestrial vegetation adaptively self-organizes to shape its own climatic conditions is still an open question, it is still possible to simulate a best case scenario, in which terrestrial gross primary productivity is periodically maximized with respect to several macroscopic vegetation parameters using an evolutionary algorithm. This is the focus of this thesis. The results of this dynamically optimized simulation are compared to a simulation where the vegetation parameters are held static at the values optimized for pre-industrial conditions. The range of uncertainty, the degree to which terrestrial productivity may be underestimated when vegetation parameterizations remain static compared to those reflecting optimal adaptation to new conditions, is quantified.

The following methods section contains a brief description of the Earth system model, more detailed descriptions of the dynamic vegetation model and the optimization algorithm, and as well as the experiments. In section 3, the results of

the sensitivity simulations and a comparison of the two transient scenarios are presented. The limitations of the methodology and ideas for future work are discussed in section 4. A brief summary and some concluding thoughts are given in the final section.

Chapter 2

Methods

2.1 Planet Simulator

The Planet Simulator (Lunkeit et al. 2004, Fraedrich et al. 2005b) is a coupled dynamic vegetation-climate system model of intermediate complexity and has been used successfully in previous studies of climate-vegetation interactions (e.g. Kleidon et al. 2000, Kleidon 2004b, Fraedrich et al. 2005a). The atmospheric component runs at a coarse resolution and has five vertical layers. It includes a dynamic core for simulating atmospheric motion and physical parameterizations of the atmospheric water cycle, clouds, and radiative transfer. The atmospheric component is coupled to a simple land surface scheme, a slab mixed-layer ocean model, and a thermodynamic sea-ice model. The land surface scheme includes a snow model, a "bucket" soil hydrology model, and a five layer soil temperature model. The large-scale land surface parameters are provided by a simplified dynamic global vegetation model (SimBA).

In its standard configuration, all model components run a horizontal grid resolution of 5.6 degrees latitude/longitude and with a time step of 45 minutes. The intermediate complexity of the Planet Simulator allows it to realistically capture the broad global patterns of climate and vegetation (see Fig. 2.1), while still running very quickly, even on a standard desktop computer. This tradeoff between

model speed and accuracy is necessary in order to make feasible the large number of simulations described later in this chapter in subsection 2.4. The standard version of the model is open source and available for download at http://www.mi.uni-hamburg.de/plasim.

2.2 SimBA

SimBA (SIMulator of Biospheric Aspects) is a simple dynamic vegetation scheme embedded within Planet Simulator, which provides the large-scale land surface parameters that are strongly influenced by terrestrial vegetation to the Planet Simulator GCM. These parameters, including land surface albedo α_s, the surface roughness length $z0_{srf}$, canopy conductance, and the soil water holding capacity of the rooting zone W_{max}, are derived from the vegetation biomass C_{veg}, the main state variable of SimBA.

Equation 2.1 describes the time evolution of C_{veg}, which is calculated as the balance of gross primary productivity (GPP), autotrophic respiration (RES_a), and litter production.

$$\frac{d\mathrm{C}_{veg}}{dt} = GPP - RES_a - \frac{\mathrm{C}_{veg}}{\tau_{veg}} \tag{2.1}$$

Autotrophic respiration is assumed to be proportional to gross primary productivity such that $RES_a = 0.5 * GPP$. This is a commonly observed ratio that has been shown to vary only slightly over a wide range of temperature and other environmental conditions at the time scales under consideration in this study (Lenton and Huntingford 2003, Waring et al 1998). Dewar (1996) argues that this con-

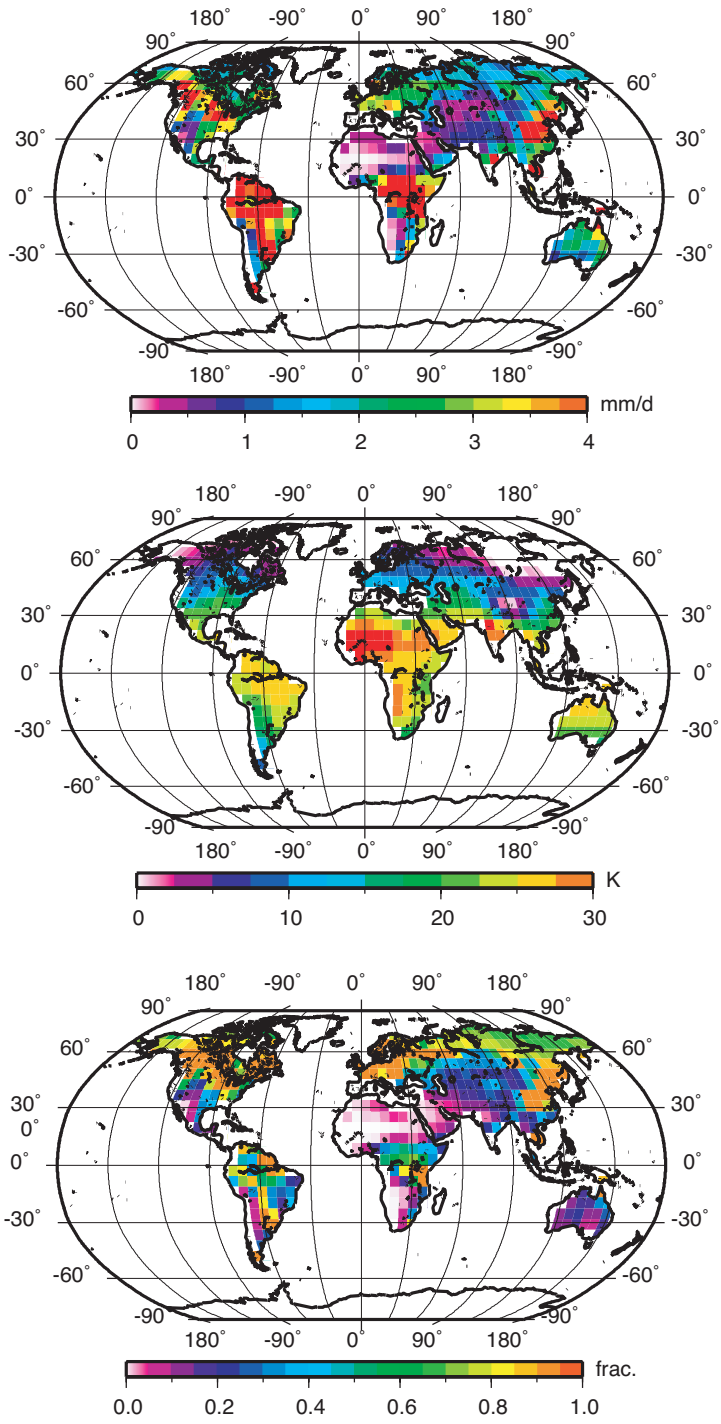

Figure 2.1: Example of Planet Simulator steady-state surface climatology run in the control setup. Annual mean plots of precipitation (top), near surface temperature (middle), and fractional leaf cover (bottom).

stant NPP/GPP ratio can be explained by optimum nitrogen allocation throughout canopies. Litter production is characterized by a mean residence time, τ_{veg}, fixed at 10 years. Together, these assumptions result in the mean vegetation biomass being proportional to mean productivity within the model.

Following Monteith et al. (1989), Dewar (1997), and Kleidon (2004), GPP is expressed as the minimum of a light-limited rate and a flux-limited rate . The light-limited rate GPP_{light} is parameterized as a multiplicative function of photosynthetically active radiation Q_{PAR}, a light use efficiency scalar ϵ_{lue}, and the fraction of the surface covered by leaves, f_{leaf}:

$$GPP_{light} \;=\; \epsilon_{lue} \;\cdot\; f_{leaf} \;\cdot\; Q_{PAR} \tag{2.2}$$

The flux-limited rate GPP_{flux} is dependent upon the CO2 gradient across the leaf-air interface and transpiration rate, ET.

$$GPP_{flux} \;=\; c \;\cdot\; \frac{p\mathrm{CO2}_{,air} \;-\; p\mathrm{CO2}_{,leaf}}{q_{\mathrm{sat}}\left(T_s\right) \;-\; q_{air}} \;\cdot\; ET \tag{2.3}$$

Bare soil evaporation and water intercepted in the canopy are not included for the sake of simplicity. Hence, the evaporative flux from the land surface is determined entirely by vegetation form and functioning. The model includes a bulk-formula evapotranspiration parameterization that takes in to account soil moisture stress and the effect of surface roughness on turbulent exchange with the overlying atmosphere. This bulk-formula parameterization of evapotranspiration is then scaled by a unitless maximum stomatal conductance parameter, gs_{max} In the standard setup of the model, gs_{max}=1, which in the absence of soil moisture stress is equivalent to

simulating the canopy as a wet surface.

The vegetation biomass C_{veg} is split between an aboveground pool $C_{veg,above}$ and a belowground pool $C_{veg,below}$ by the prescribed root-shoot partitioning parameter p_{rs}:

$$\mathrm{C}_{veg,above} \;=\; \mathrm{C}_{veg} \;\cdot\; p_{rs} \tag{2.4}$$

and

$$\mathrm{C}_{veg,below} \;=\; \mathrm{C}_{veg} \;\cdot\; (1 \;-\; p_{rs}) \tag{2.5}$$

These two parameters are converted in to fractional covers of aboveground and belowground vegetation by

$$f_{veg,above} \;=\; \frac{1}{c_c} \;\cdot \arctan\left(\frac{2 \;\cdot\; \mathrm{C}_{veg,above} \;-\; c_a}{c_b}\right) \;+\; c_d \tag{2.6}$$

and

$$f_{veg,below} \;=\; \frac{1}{c_c} \;\cdot \arctan\left(\frac{2 \;\cdot\; \mathrm{C}_{veg,below} \;-\; c_a}{c_b}\right) \;+\; c_d \tag{2.7}$$

where c_a , c_b , c_c , and c_d are empirical parameters that were derived from observations to match the transition of forested to non-forested vegetation along climatic gradients. The proportion of the surface covered by green leaves, f_{leaf}, is calculated as a function of leaf area index (LAI) by

$$f_{leaf} \;=\; 1 \;-\; \exp\;(-k \;\cdot\; LAI) \tag{2.8}$$

where $k = 0.5$.

These fractional covers are used to express land surface properties as functions of relative proportion of grid cell area that is fully vegetated to bare, non-vegetated surface. The surface roughness length $z0_{srf}$ is calculated from the fractional cover of forest fveg,above by:

$$z_{0,srf} \;=\; z_{0,veg} \;\cdot\; f_{veg,above} \;+\; z_{0,noveg} \;\cdot\; (1 \;-\; f_{veg,above}) \tag{2.9}$$

where the roughness of a bare surface $z0_{nonveg} = 0.05$ m and the vegetation roughness $z0_{veg}$ is an externally prescribed parameter. Take notice that in this parameterization, $z0_{veg}$ is scaled to the fractional cover of aboveground vegetation and thus represents the maximum vegetation roughness length. Overall surface roughness is derived by combining the orographic roughness $z0_{oro}$ with the land surface roughness $z0_{srf}$ using:

$$z_0 \;=\; \left(z_{0,oro}^2 \;+\; z_{0,srf}^2\right)^{\frac{1}{2}} \tag{2.10}$$

The influence of the surface roughness calculated in Eqn. 2.10 on bulk evapotranspiration is described in Section 2.1 of Lunkeit et al (2004).

The maximum soil water content of the rooting zone W_{max} is derived in a similar fashion from $f_{veg,below}$ by

$$W_{\max} \;=\; W_{\max,veg} \;\cdot\; f_{veg} \;+\; W_{\max,nonveg} \;\cdot\; (1 - f_{veg,below}) \tag{2.11}$$

where $W_{max,nonveg} = 50$ mm, $W_{max,veg} = 500$ mm (taken as a typical value from Kleidon 2004c) are the corresponding values for a bare and fully vegetated surface respectively.

2.3 Optimization Algorithm

The optimization technique used in this study is adapted from the macroevolutionary algorithm (MA) first described by Marin and Sole (1999). Macroevolutionary algorithms differ from genetic algorithms, a more commonly known class of evolutionary algorithms, in that instead of relying on a population-level metaphor, they exploit a metaphor based on evolution at higher taxa level where extinction and diversification are the primary drivers (Marin and Sole 1999). A macroevolutionary algorithm was chosen over a standard genetic algorithm because it has been shown that MA's are able to search faster over a solution space even with a very small population of candidate solutions (Marin and Sole 1999, Zhang and Xu 2005). This was an important consideration because the number of candidate solution simulations that could be conducted in parallel at each generation of the iteration was limited by the available computing resources.

The optimization algorithm iterates over a number of generations G. In the original MA described by Marin and Sole (1999), each generation constitutes a set of P species (candidate solutions) where each P_i consists of a vector of input parameters. In this setup, each of the P_i describes a model run. However, here each P_i is described by a 2048×2 array of input parameters containing the biotic parameter values, $z_{0,max}$ and gs_{max}, for every grid cell of the model. Each grid cell (row of P_i), can then can be described as a 2-vector $X_{i,n}$ (gs_i , z_{0i}) where n denotes the specific grid cell. The values for ocean grid cells are set to zero.

The simulations are run for a number of years and afterwards the fitness value

$f\left(X_{i,n}\right)$, the mean gross primary productivity over the length of the simulation, is computed for each grid cell. This fitness value is used in the calculation of a connectivity matrix W for each grid cell. Each entry in the connectivity matrix W is a measure of the influence of species j on species i at generation t normalized to a continuous value within the range between -1 and 1. $W_{i,j,n}$ is defined as

$$W_{i,j,n} \;=\; \frac{f\left(X_{i,n}\right) \;-\; f\left(X_{j,n}\right)}{\mid X_{i,n} \;-\; X_{j,n} \mid} \tag{2.12}$$

where the numerator is the distance in fitness space between species and the denominator is the distance in parameter space. In cases where the denominator is zero, $W_{i,j,n}$ is set to 0. The distances in parameter space are normalized to a range of $[0, 1]$ as not to give undue weight to the canopy roughness parameter.

The survival coefficient h at each grid cell n for each species i is then computed as given by

$$h_{i,n}\;\left(t\right) \;=\; \sum_{j=1}^{P} W_{i,j,n}\;\left(t\right) \tag{2.13}$$

where t is the generation number. If $h_{i,n} \leq 0$ then the grid cell $X_{i,n}$ is said to be extinct and its values discarded. Extinct sites are then filled in two ways. With probability τ, a completely new solution for $X_{i,n}$ is randomly generated within the bounds of the biota parameter fields. Otherwise with probability $1 \;-\; \tau$, the extinct grid cell $X_{i,n}$ is colonized with a value from a randomly chosen surviving grid cell $X_{j,n}$. The colonized grid cell value is then altered slightly by adding a small random value between $[-\epsilon, \epsilon]$. If an altered value lies outside the parameter boundaries, the new value is set to nearest parameter limit. The parameter τ decreases with each

generation as in simulated annealing as given by

$$\tau\left(t\right) \;=\; \max\left(0.2 \;-\; \frac{t}{200},\; 0.01\right) \tag{2.14}$$

.

2.4 Experimental Design

2.4.1 Steady State Simulations

An array of sensitivity simulations were conducted over a range of parameter values for maximum stomatal conductance gs_{max}, canopy roughness $z0_{veg}$ and root-shoot partitioning p_{rs}. In these sensitivity simulations, the parameters were prescribed uniformly across all land grid cells. Simulations were conducted for gs-max values of 0.01, 0.02, 0.05, 0.1, 0.2, 0.3, 0.4, 0.5, and 1.0; $z0_{veg}$ values of 0.1, 0.2, 0.5, 1, 2, 5 and 10; and p_{rs} values of 0.01, 0.1, 0.3, 0.5, 0.7, 0.9, and 0.99. The "Control" simulation was represented by $gs_{max} = 1.0$, $z0_{veg}$= 2.0, and $p_{rs} = 0.5$, the parameter values used in the standard configuration of the model.

The simulations were run for the equivalent of 200 years with prescribed, climatological sea-surface temperatures and sea-ice cover to allow the coupled dynamic vegetation-climate system to reach a steady state. The last 10 years of model output from each simulation were averaged for the analysis. The atmospheric carbon dioxide concentration was fixed at 360 ppm. Some simulations with high values for canopy roughness and stomatal conductance were run with the time step reduced by half to ensure numerical stability.

The partitioning of the land surface fluxes found in the sensitivity simulations was compared to observations from the ECMWF ERA-40 climate reanalysis (Uppalla 2005). The ERA-40 reanalysis consists of global meteorological data on a 2.5° x 2.5° grid for the period of 1957 to 2002 based on a reanalysis of observations from multiple platforms. For the purposes of this experiment, the monthly temperature and land surface flux data were extracted from the ERA-40 reanalysis for the period of 1980 to 1989. This comparison of the fluxes was performed at the vegetation-type/biome scale. Since the SimBA model does not use vegetation biomes per se, the simulated control climate was used in conjunction with the BIOME classification model (Prentice et al. 1992) to derive biome masks corresponding to the various vegetation types. The BIOME model was used to predict which vegetation types (biomes) would be dominant in each grid cell of the simulated control climate based on the monthly mean values of precipitation, temperature, and soil moisture stress. Due to the relatively coarse resolution of the Planet Simulator, in some cases, there were very few grid cells in a biome mask produced by the BIOME model. This was overcome by merging some of the biomes from the BIOME model; the tropical rainforest and tropical seasonal forest became 'tropical forest', warm mixed forest and temperate deciduous forest became 'temperate forest', and cool mixed forest, cool conifer forest, and taiga became 'boreal forest'. The other biome masks produced by the BIOME model were not used in the analysis. Using these masks, the surface fluxes from the sensitivity climates were averaged over the different biomes. The same process was repeated to derive the corresponding biome-averaged surface fluxes from the ECMWF ERA-40 climate reanalysis data.

2.4.2 Transient Simulations

Two transient scenarios were simulated for the period 1850-2100 with prescribed historical and projected atmospheric CO2 concentrations representing an 'optimizing' scenario (optimal adaptation) and a 'static scenario' (no adaptation). In the transient scenarios, the model was run with the slab mixed-layer ocean model and the thermodynamic sea-ice model. This was necessary to adequately simulate the water vapor feedback over the range of simulated greenhouse conditions. In the spinup process, the model was run with a prescribed pre-industrial CO2 concentration of 280 ppm until the vegetation biomass and soil carbon pools arrived at steady states. The gs_{max} and $z0_{veg}$ parameter sets were then optimized over 20 generations of the MA using a population of nine species. The root-shoot partitioning parameter, p_{rs}, was not optimized. In preliminary testing, the productivity was found to be least sensitive to the optimization of the root-shoot parameter. Each parameter to be optimized increases the computational burden exponential. This root-shoot parameter was excluded to allow the optimizations to be run to completion within time constraints. In the sensitivity simulations, the model output was least sensitive to this parameter and it was excluded to increase the speed of the optimization process.

In the 'static' scenario, the model was run from 1850 to 2100 with increasing prescribed CO2 concentrations following historical and projected values in the Post-SRES A2 scenario obtained from Schlesinger and Malyshev (2001). The vegetation parameters, optimized for a pre-industrial CO2 concentration of 280 ppm during

the spin up process, were not changed during the course of the simulation period. This scenario represents a "worst case" in which there is no large-scale, climatically relevant adaptation by terrestrial vegetation in terms of maximum stomatal conductance or canopy roughness.

In the 'optimizing' scenario, the model was run from 1850 to 2100 following the same prescribed CO2 trajectory as in the 'static' scenario. However, the gs_{max} and $z0_{veg}$ parameters were periodically optimized at each grid cell using the MA during the years 1970-1972, 2000-2002, 2020-2022, 2040-2042, 2060-2062, and 2080-2082. The vegetation parameters were optimized over 20 generations using a population of nine species. This scenario represents a "best case" in which terrestrial vegetation adapts optimally at the large, climatically relevant scale in terms of maximum stomatal conductance or canopy roughness.

During the period of 1970 to 1972, for instance, nine model runs were intialized in the first generation of the optimization with the model restart files from the end of 1969. One of these runs used the gs_{max} and $z0_{veg}$ parameter values from the period 1860 to 1969. The other eight runs used differing prescribed sets of vegetation parameter values. Following the MA, the results of this first generation were processed and nine new sets of vegetation parameters were created for the second generation. The optimization process was repeated for twenty generations. Out of the resulting 180 runs, the set of vegetation parameters resulting in the highest global mean GPP during the three year period was used to initialize the model for the year 1973. The model was then run from 1973 to 1999 and in the year 2000 the process began again.

Chapter 3

Results

In this section, the results of the the two modelling experiments are presented. In the first section, the range of biologically possible climate-vegetation steady states are quantified in terms of the annual mean land surface boundary conditions averaged over all land areas and over the tropical forest, temperate, and boreal biomes. Then, the characteristic partitioning of the energy fluxes at the land surface are then compared to observations found in the ECMWF ERA-40 reanalysis (Upsalla 2005) to test whether present-day climatic conditions are near optimal in terms of biospheric functioning. In the second section, the range of uncertainty in terrestrial productivity is quantified, over the course of the 250 year transient simulation period, between the "optimizing" scenario, in which vegetation properties periodically adapt to a new optimum, and the "static" scenario, in which vegetation properties remained fixed at optimum conditions for pre-industrial conditions. The geographic pattern of differences between the two scenarios in terms of vegetation properties, terrestrial productivity and biomass, and climatic conditions are compared at year 2100.

3.1 Sensitivity Simulations

3.1.1 Possible Range of Steady States

The results of the sensitivity simulations are shown in terms of land surface boundary conditions (precipitation and surface air temperature) averaged by biome in Figure 2.1. Note that each box represents the biome-average values of precipitation and surface temperature for a single sensitivity simulation and the shading denotes the simulated gross primary productivity. These simulations show a general trend of higher productivity where the set of values for the model parameters characterizing vegetation form and functioning led to a climatic regime with lower temperatures and greater rates of precipitation. In all three plots, the boundary conditions of the control simulations are largely consistent with the sensitivity simulations associated with optimal conditions for productivity. The parameters values of gs_{max} and $z0_{veg}$ that resulted in the highest mean productivity were 0.1 and 0.5m for the tropical forest biome, 0.2 and 2.0m for the temperate biome, and 0.1 and 1.0m for the boreal biome. In the plot of the tropical biome, the optimal sensitivity climates, the control simulation, and the ECMWF reanalysis values correspond remarkably well. More importantly, these plots confirm that vegetation adds a great deal of flexibility to land surface functioning; allowing for many possible climate-vegetation steady states which differ greatly in their gross primary productivity.

3.1.2 Energy Flux Partitioning

Figure 2.2 shows the results from the same sensitivity simulations in a similar fashion in terms of the turbulent fraction, the partitioning between radiative and turbulent fluxes ($Q_{LH} + Q_{SH}/Q_{SW}$), averaged over the biome regions. Table 1 shows the values for turbulent fraction from the sensitivity simulation with the optimum set of vegetation parameter values, the control simulation, and the corresponding observed values from the ECMWF reanalysis for each biome region. The optimum set of vegetation parameter values being defined here as those which led to the highest mean gross primary productivity for that particular biome.

It was found to be useful to compare the characteristic partitioning of fluxes rather than absolute fluxes due to biases in the energy balance inherent to the Planet Simulator model. For instance, in the boreal region, the Planet Simulator underestimates the presence of clouds, which leads to an underestimation of net solar radiation and surface temperatures.The values of turbulent fraction found in the sensitivity climates with the highest gross primary productivities are largely consistent with the observed values in the ERA-40 reanalysis. Overall, it appears that the highest simulated productivities fall close to but not at the upper limit of the simulated range of turbulent to radiative flux ratios. These results add support to the hypothesis that vegetation productivity is at its maximum possible value within the climate system, given the constraints of the surface energy and water balance.

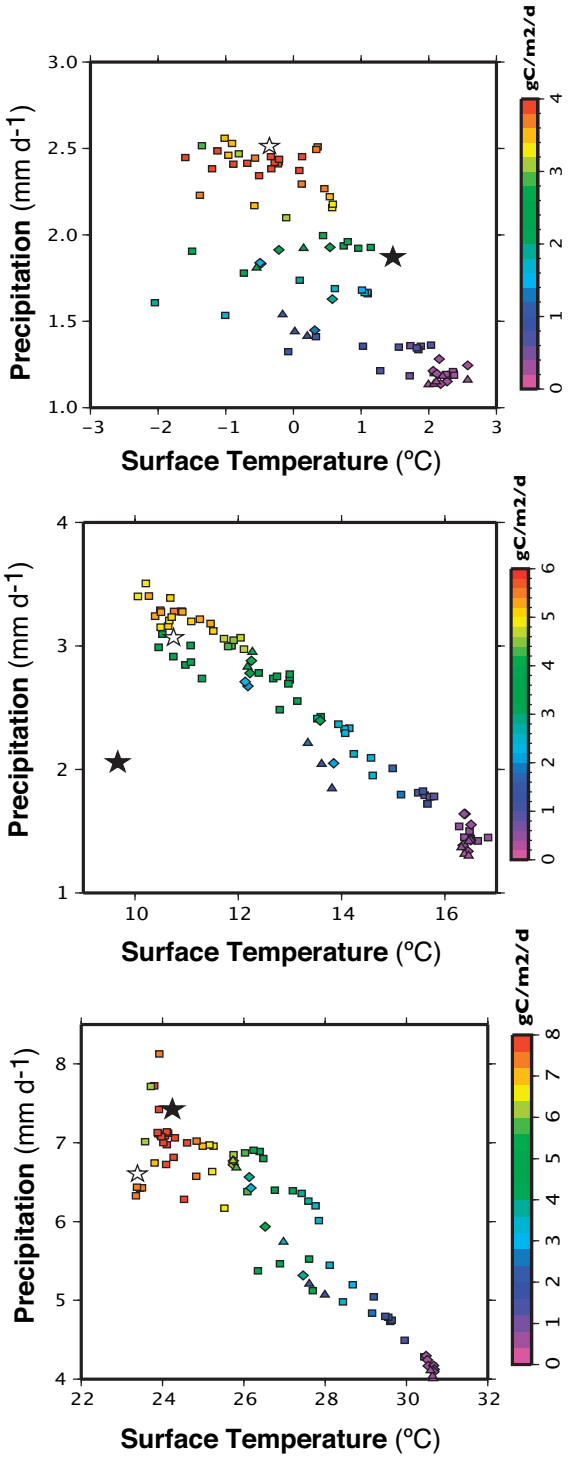

Figure 3.1: Climatic mean land surface boundary conditions averaged for the boreal (top), temperate (middle), and tropical (bottom) biomes. Each box represents a single sensitivity simulation and the shading denotes the simulated productivity. The white star represents the control simulation and the black star marks the boundary conditions found in the ECMWF ERA-40 reanalysis.

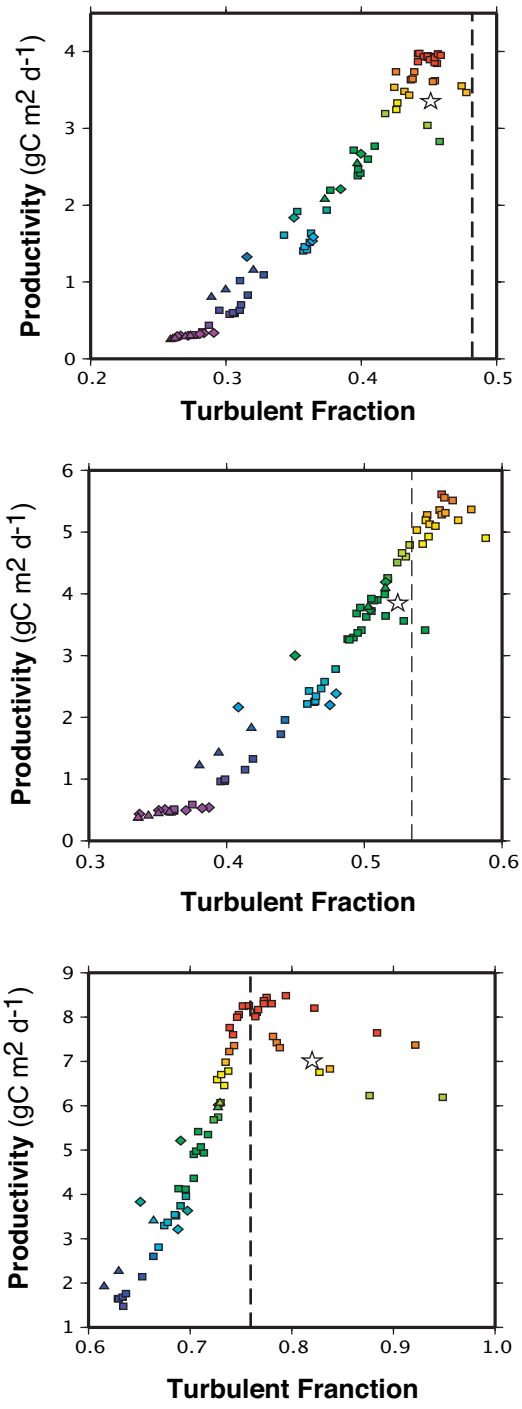

Figure 3.2: Partitioning of radiative to turbulent energy fluxes averaged for the boreal (top), temperate (middle), and tropical (bottom) biomes. Each box represents a single sensitivity simulation and the shading denotes the simulated productivity. The white star represents the control simulation and the dashed vertical line marks the partitioning found in the ECMWF ERA-40 reanalysis.

3.2 Transient Simulations

3.2.1 Range of Uncertainty in Simulated Future Terrestrial Productivity

Figure 3.3 (top) shows the change in annual mean gross primary productivity over the course of the "optimizing" and "static" scenarios. The difference between the two scenarios represents the range of uncertainty in terrestrial productivity between no adaptation in terms of the macroscopic vegetation properties and optimal adaptation leading to maximized productivity. In both scenarios, the CO2 fertilization effect lead to an increase in GPP and an accumulation of vegetation biomass. After the first optimization period from 1970 to 1973, the GPP in the 'optimizing' scenario begins to increase at a faster rate than the the 'static' simulation for a few years. Shortly thereafter, the difference between the two scenarios disappeared again . The range between the two scenarios grew during each subsequent optimization period. However, in some of the spans between the optimizations, the rate of increase in GPP is higher in the 'static' scenario than the 'optimizing' scenarios. Most drastically, in the period 2083 to 2100, the GPP in the 'static scenario' is nearly matches the productivity in the 'optimizing' scenario.

Figure 3.3 (bottom) shows the change in vegetation biomass over the same period of 1850 to 2100. In the Planet Simulator, mean biomass is proportional to mean gross primary productivity. Therefore, comparing the evolution of vegetation carbon pools reveals the cumulative effect of changes in GPP and with less interannual

variability.The total increase in vegetation carbon from 1850 to 2100 was about 251 PgC in the 'static' scenario and 273 PgC in the 'optimizing' scenario. The periodic optimization of the gsmax and z0,veg parameter values led to the accumulation of about 22 PgC more in the vegetation carbon pool at year 2100 in the 'optimizing' scenario than in the 'static scenario'. The largest difference in vegetation biomass of about 28 PgC occurred at year 2083 after the last optimization period from year 2080 to 2083.

3.2.2 Geographic Differences Between Optimized and Static Simulations

The spatial differences between the two scenarios at year 2100 in terrestrial gross primary productivity and terrestrial biomass are shown in Figure 3.4. The 'optimizing' scenario' saw significantly larger gains in GPP and biomass in northern Australia, southeast Asia, southern Africa, and the northern latitudes. In central United States and the tropical forest regions of eastern Amazonia and Central Africa, there were significantly larger gains in GPP and biomass in the 'static' scenario. This indicates that while the optimization algorithm led to a higher mean global productivity, it failed to optimize the vegetation parameters across all regions.

Figure 3.5 shows the geographic differences in the vegetation parameters, gs_{max} and $z0_{veg}$, between the two scenarios after the final optimization period. The optimization algorithm led to a decrease in maximum stomatal conductance parameter values in most vegetated regions of the world. The decreases in maximum stomatal

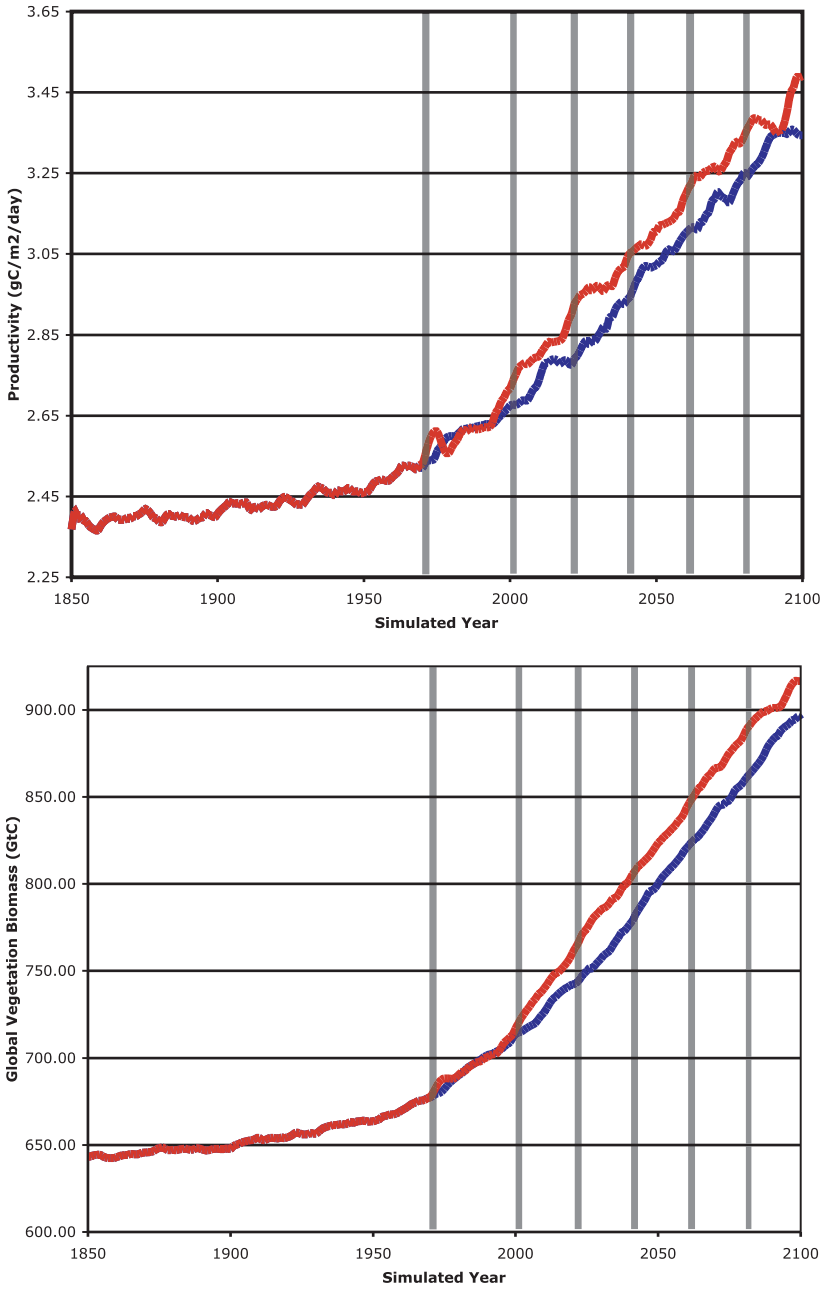

Figure 3.3: Time evolution of terrestrial productivity (top) and vegetation biomass (bottom). The red line is from optimizing scenario and the blue line represents the static scenario.

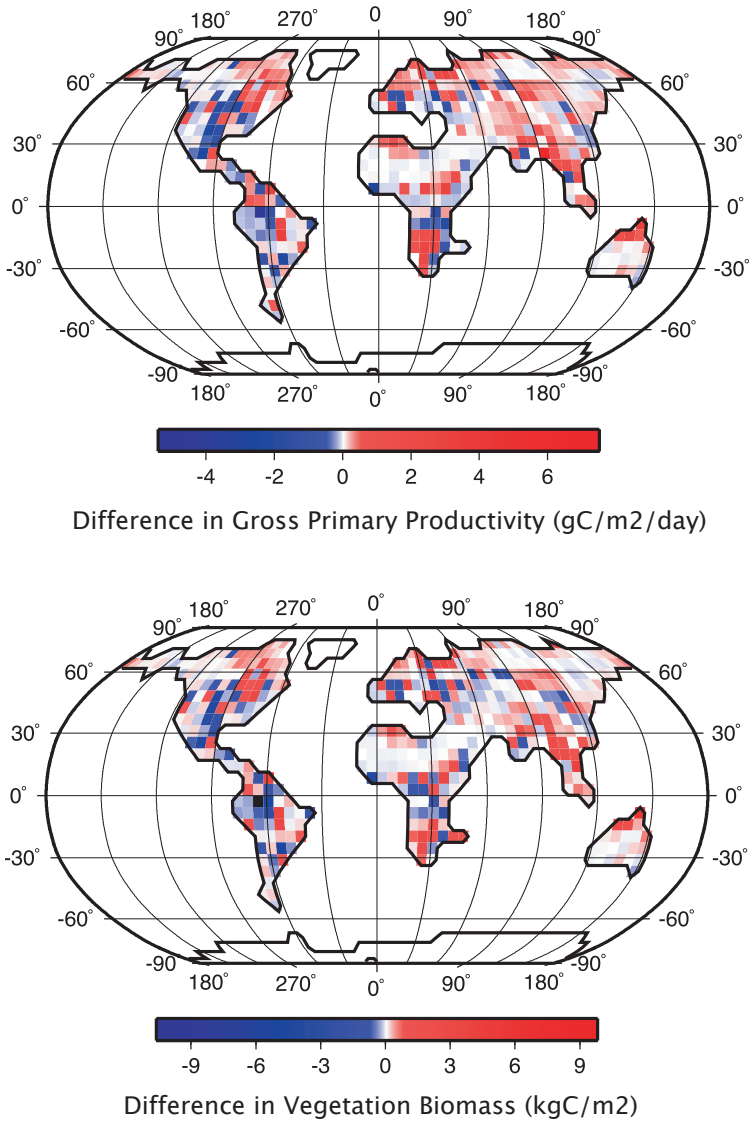

Figure 3.4: Differences between the static and optimizing scenarios in gross primary productivity (top) and vegetation biomass (bottom) at year 2100

conductance was most pronounced in the tropics and the northern latitudes. This is consistent with the observed reduction in stomatal density reported in Woodward (1989).

There is no similarly consistent spatial pattern of differences in the roughness parameter values between the scenarios. There were marked decreases in roughness in northern Australia and southern Africa. The magnitude of differences in roughness lengths were generally greater than the magnitude of differences in maximum stomatal conductance. However, this does not suggest that the impact of changes in roughness length are greater than the impact of changes in maximum stomatal conductance because stomatal conductance has much a greater influence on the turbulent mass and energy exchange at the atmosphere-biosphere boundary.

Figure 7 shows the geographic pattern of differences at year 2100 between the two scenarios in turbulent fraction. A positive difference in turbulent fraction means that the turbulent fluxes increased at the expense of radiative cooling. There is a strong negative signal in Africa, especially east Africa and south Africa. There are also decreases in northern Australia, southeast Asia, and Indonesia.

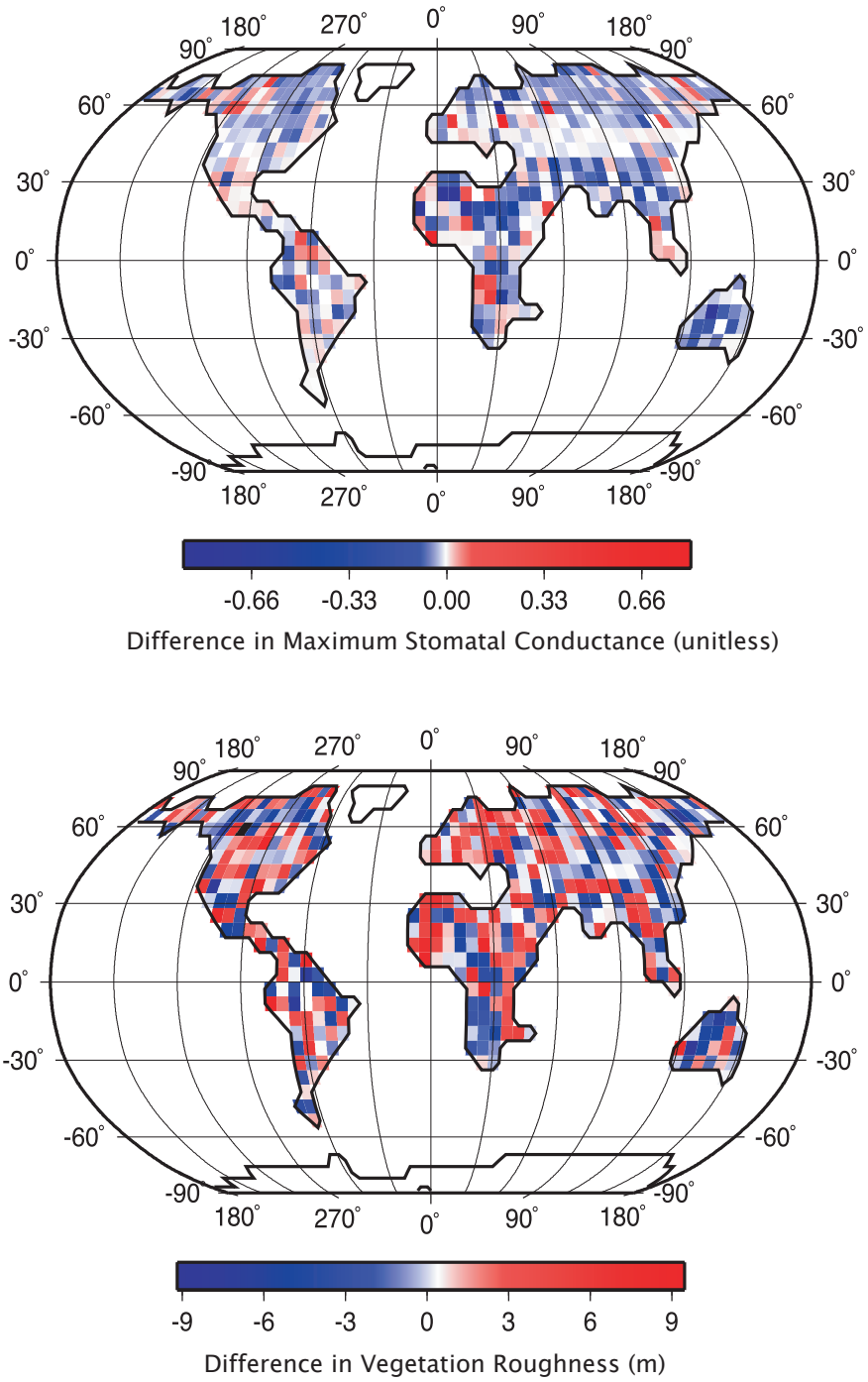

Figure 3.5: Differences between the static and optimizing scenarios in maximum stomatal conductance (top) and vegetation roughness (bottom) at year 2100

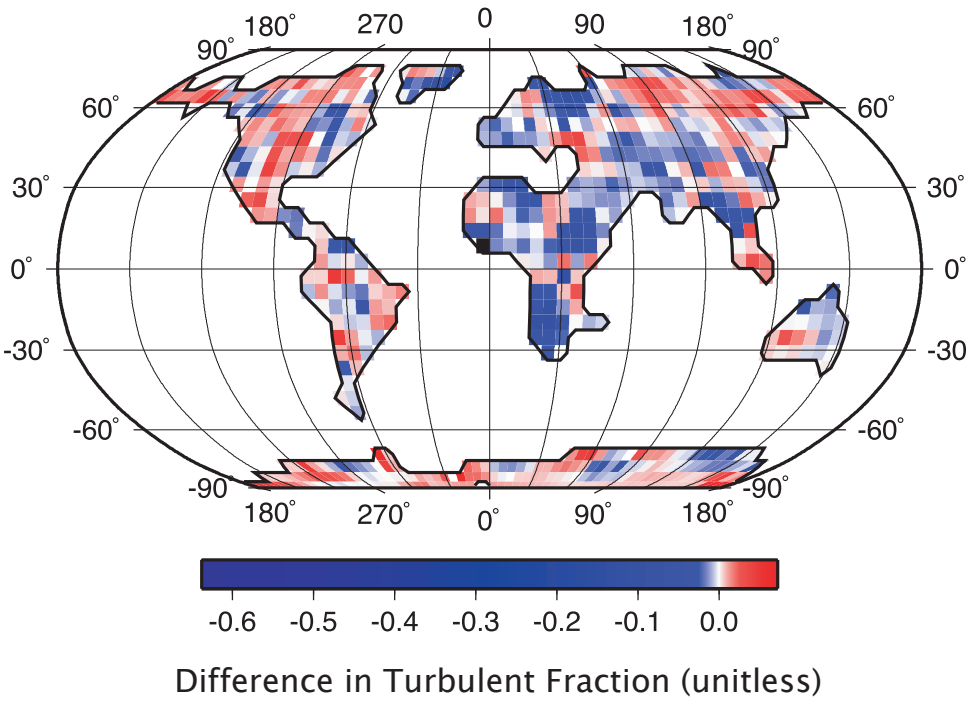

Figure 3.6: Differences between the static and optimizing scenarios in turbulent fraction at year 2100

Chapter 4

Discussion

4.1 Limitations of Model and Experimental Setup

The Planet Simulator is a model of intermediate complexity, and thus, many climate and vegetation processes are ignored or highly simplified. The simulations were performed at a fairly coarse horizontal and vertical resolutions. The model does not include nutrients as a limiting factor on productivity and the soil hydrology scheme includes only one layer. In the sensitivity study, the vegetation parameters were varied in a globally uniform manner in the sensitivity simulations. While this simplifies the analysis, a more realistic approach for estimating the range of possible steady states might use a cloud of randomly generated, spatially heterogeneous parameter sets. Also, climatological sea-surface temperatures and sea-ice extents were externally prescribed in the sensitivity study. Bonan et al (1992) presents the potential interactions between the springtime warming associated with a darker vegetated boreal forest and oceanic and sea-ice feedbacks. This sort of land-sea interaction would not be captured in the described sensitivity experiment.

Both the transient and sensitivity simulations were performed with prescribed CO2 concentrations, making it impossible to directly compare the results of this study with other carbon-climate feedback studies mentioned in Section 1.3. This study should be extended using a fully interactive carbon model with feedbacks

to the atmosphere and including the nutrient demands of vegetation. Additional model parameters, such as leaf albedo and stomatal response to vapor pressure deficits, could also be included in the optimization.

4.2 Performance of the Optimization Algorithm

The optimization algorithm as implemented in this study performed poorly. By definition, an optimized set of parameters should produce productivity values which are greater than or at least equal to the static parameters. In the optimizing scenario presented here, each optimization period caused an initial gain in productivity over the static scenario. However, in the interim periods between optimizations, these gains were not sustained with the global productivity of the optimized scenario falling below the static scenario. Repeating the study with a longer optimization (e.g. 10 years) may improve the results by allowing the simulated land surface more time to approach a new equilibrium. The algorithm also performed poorly in some key areas including Amazonia resulting in an overall lower biomass in those region at the end of the optimization scenario when compared to the static scenario. Running the optimizations requires a considerable amount of time even with a moderate-size cluster of computational nodes. Nonetheless, a systematic approach examining the tradeoffs between the length of the optimization period, the frequency of optimizations, the number of generations per optimization, the required computational burden, and the effectiveness of the algorithm would be a useful project and greatly improve the credibility of any results developed using the methodology

presented for the first time in this study. Unfortunately, this was not feasible within the timeframe of this study. Additionally, the use of other optimization algorithms such as gradient-based and extremal optimization methods, as well as variants of the one presented in this paper should be explored.

Chapter 5

Conclusion

This study shows that vegetation adds a great deal of flexibility to the land surface allowing for a wide range of biologically possible climate-vegetation states that differ in their productivity. This suggests that the energy and mass balances do not determine but only act to constrain the emergent state of the climate-vegetation system. Furthermore, the partitioning of radiative to turbulent fluxes found in the sensitivity simulations with the highest productivities is largely consistent with observations from the ERA-40 reanalysis. This is consistent with the hypothesis that the present-day climate reflects optimal conditions for the terrestrial biosphere due in part to form and functioning of the biosphere itself.

A new methodology was presented to quantify the range of uncertainty in future terrestrial productivity associated with potential adaptation of large-scale, climatically relevant vegetation properties. Under scenarios of global change, these large-scale vegetation properties may adapt to a new configuration that maintains an optimum partitioning of surface fluxes leading to a state of maximum productivity for the new conditions. In which case, a selection criterion will be necessary to pick out the this state from the range of possible climate-vegetation states. An optimization approach may be a valuable tool for selecting from the many possible steady states.

Even if the terrestrial biosphere is unable to consistently maintain, through large-scale feedbacks, optimum conditions for productivity, the methodology of investigating past and future climate change from the perspective of optimality provides an important quantification of a best case scenario. This is of particular relevance as current research on future climate change is focused on positive feedbacks and negative impacts on the terrestrial biosphere (e.g. Cox et al. 2000, Friedlingstein et al. 2003), while optimality provides the complementary perspective of the best case climate change scenario and emphasizes the dominance of negative feedbacks.

Bibliography

[1] R. A. Betts. Self-beneficial effects of vegetation on climate in a ocean-atmosphere general circulation model. *Geophys. Res. Lett.*, 26:1457–1960, 1999.

[2] R. A. Betts, P. M. Cox, S. E. Lee, and F. I. Woodward. Contrasting physiological and structural vegetation feedbacks in climate change simulations. *Nature*, 387:796–799, 1997.

[3] G. B. Bonan, D. Pollard, and S. L. Thompson. Effects of boreal forest vegetation on global climate. *Nature*, 359:716–718, 1992.

[4] G.B. Bonan. *Ecological climatology : concepts and applications*. Cambridge University Press, 2002.

[5] M. Claussen and V. Gayler. The greening of the sahara during the mid-holocene: Results of an interactive atmosphere-biome model. *Global Ecology and Biogeography Letters*, 6(369-377), 1997.

[6] I. R. Cowan. Stomatal behaviour and environment. *Adv. Bot. Res.*, 4:117–128, 1977.

[7] P.M. Cox, R. A. Betts, C.D. Jones, S.A. Spall, and I.J. Totterdell. Acceleration of global warming due to carbon-cycle feedbacks in a coupled-climate model. *Nature*, 408(184-187), 2000.

[8] N.I. de Noblet, I.C. Prentice, S. Joussaume, D. Texier, A. Botta, and A. Haxeltine. Possible role of atmosphere-biosphere interactions in triggering the last glaciation. *Geophys. Res. Lett.*, 23:3191–3194, 1996.

[9] R. C. Dewar. A root-shoot partitioning model based on carbon-nitrogen-water interactions and munch phloem flow. *Funct. Ecol.*, 7:356–368, 1993.

[10] R. C. Dewar. The correlation between plant growth and intercepted radiation: An interpretation in terms of optimal plant nitrogen content. *Annals of Botany*, 78:125–136, 1996.

[11] R. C. Dewar. A simple model of light and water use efficiency for pinus radiata. *Tree Physiology*, 17:259–265, 1997.

[12] R. C. Dewar. Information theory explanation of the fluctuation theorem, Maximum Entropy Production, and self-organized criticality in non-equilibrium stationary states. *J. Physics A*, 36:631–641, 2003.

[13] R. C. Dewar. Maximum entropy production and non-equilibrium statistical mechanics. In A. Kleidon and R. D. Lorenz, editors, *Non-Equilibrium Thermodynamics and the Production of Entropy: Life, Earth, and Beyond*. Springer Verlag, Heidelberg, Germany, 2005.

[14] R. C. Dewar. Maximum entropy production and the fluctuation theorem. *J. Physics A*, 38:L371–L381, 2005.

[15] P.S. Eagleson. *Ecohydrology: Darwinina expresion of vegetation form and function*. Cambridge University Press, New York, 2002.

[16] C.B. Field. Allocating leaf nitrogen for the maximization of carbon gain: leaf age as a control on the allocation program. *Oecologica*, 56:341–347, 1983.

[17] C.B. Field, M.J. Behrenfeld, J.T. Randerson, and P. Falkowski. Primary production of the biosphere: Integrating terrestrial and oceanic components. *Science*, 281:237–240, July 1998.

[18] J. A. Foley, J.E. Kutzbach, M.T. Coe, and S. Levis. Feedbacks between climate and boreal forests during the holocene epoch. *Nature*, 371:52–54, 1994.

[19] K. Fraedrich, H. Jansen, E. Kirk, U. Luksch, and F. Lunkeit. The planet simulator: Towards a user friendly model. *Z. Meteorol.*, 14:299–304, 2005.

[20] K. Fraedrich, H. Jansen, E. Kirk, and F. Lunkeit. The planet simulator: Green planet and desert world. *Z. Meteorol.*, 14:305–314, 2005.

[21] P. Friedlingstein, L. Bopp, P. Ciais, J.-L. Dufresne, , L. Fairhead, H. LeTreut, P. Monfray, L. Orr, J. Fairhead, H. LeTreut, P. Monfray, and J. Orr. Positive feedback between future climate change and the carbon cycle. *Geophys. Res. Lett.*, 28:1543–1546, 2001.

[22] P. Friedlingstein, P. Cox, R. Betts, L. Bopp, W. von Bloh, V. Brovkin, P. Cadule, S. Doney, M. Eby, I. Fung, G. Bala, J. John, C. Jones, F. Joos, T. Kato, M. Kawamiya, W. Knorr, K. Lindsay, H. D. Matthews, T. Raddatz, P. Rayner, C. Reick, E. Roeckner, K. G. Schnitzler, R. Schnur, K. Strassmann, A. J. Weaver, C. Yoshikawa, and N. Zeng. Climate-carbon cycle feedback analysis: Results from the c4mip model intercomparison. *Journal of Climate*, 19:3337–3353, 2006.

[23] Cowan I.R. and Farquhar G.D. Stomatal function in relation to leaf metabolism and environment. *Symp Soc Exp Biol*, 31:471–505, 1977.

[24] A. Kleidon. Beyond Gaia: Thermodynamics of life and Earth system functioning. *Clim. Ch.*, 66:271–319, 2004.

[25] A. Kleidon. Global datasets of rooting zone depth inferred from inverse methods. *J. Clim.*, 17:2714–2722, 2004.

[26] A. Kleidon. Optimized stomatal conductance of vegetated land surfaces and its effects on simulated productivity and climate. *Geophys. Res. Lett.*, 31:L21203, 2004.

[27] A. Kleidon. Optimum stomatal conductivity, maximum photosynthesis, and regional vegetation-climate interactions: Part I: Emergence of optimality from individual-based dynamics. *Clim. Ch.*, 2004. submitted.

[28] A. Kleidon. Quantifying the biologically possible range of steady-state soil and surface climates with climate model simulations. *Biologia*, 61:S234–S239, 2006.

[29] A. Kleidon and K. Fraedrich. Biotic entropy production and global atmosphere-biosphere interactions. In A. Kleidon and R. D. Lorenz, editors, *Non-Equilibrium Thermodynamics and the Production of Entropy: Life, Earth, and Beyond*, pages 173–190. Springer Verlag, Heidelberg, Germany, 2005.

[30] A. Kleidon, K. Fraedrich, and M. Heimann. A green planet versus a desert world: Estimating the maximum effect of vegetation on land surface climate. *Clim. Ch.*, 44:471–493, 2000.

[31] A. Kleidon and M. Heimann. A method of determining rooting depth from a terrestrial biosphere model and its impacts on the global water- and carbon cycle. *Global Change Biol.*, 4:275–286, 1998.

[32] A. Kleidon and M. Heimann. Assessing the role of deep rooted vegetation in the climate system with model simulations: mechanism, comparison to observations and implications for amazonian deforestation. *Clim. Dyn.*, 16:183–199, 2000.

[33] A. Kleidon and S. Lorenz. Deep roots sustain amazonian rainforest in climate model simulations of the last ice age. *Geophys. Res. Lett.*, 28:2425–2428, 2001.

[34] G. Knorr, K. Grosfeld, G. Lohmann, F. Lunkeit, , and K. Fraedrich. Atmospheric responses to abrupt changes in the thermohaline circulation during deglaciation. *Geochemistry, Geophysics, and Geosystems*, in revision, 2005.

[35] J.E. Kutzbach, G. B. Bonan, J. A. Foley, and S.P. Harrison. Vegetation and soil feedbacks on the response of the african monsoon to orbital forcing in the early and middle holocene. *Nature*, 384(623-626), 1996.

[36] F. Lunkeit, K. Fraedrich, H. Jansen, E. Kirk, A. Kleidon, and U. Luksch. Planet simulator reference manual. available at http://puma.dkrz.de/plasim, 2004.

[37] J. L. Monteith, A. K. S. Huda, and D. Midya. Rescap: a resource capture model for sorghum and pearl millet. In S. M. Virmani, H. L. S. Tandon, and G. Alagarswamy, editors, *Modelling the growth and development of sorghum and pearl millet*, pages 30–34. ICRISAT Research Bulletin 12, Patancheru, India, 1989.

[38] I. C. Prentice, W. Cramer, S. P. Harrison, R. Leemans, R. A. Monserud, and A. M. Solomon. A global biome model based on plant physiology and dominance, soil properties and climate. *J. Biogeography*, 19:117–134, 1992.

[39] M.E. Schlesinger and S. Malyshev. Changes in near-surface temperature and sea level for the post-sres co2-stabilization scenarios. *Integrated Assessment*, 2:95–110, 2001.

[40] P. J. Sellers, S. O. Los, C. J. Tucker, C. O. Justice, D. A. Dazlich, G. J. Collatz, and D. A. Randall. A revised land surface parameterization SiB2 for atmospheric GCMs. 2. the generation of global fields of terrestrial biophysical parameters from satellite data. *J. Clim.*, 9:706–737, 1996.

[41] J. Shukla and Y. Mintz. Influence of land-surface evapotranspiration on the earth's climate. *Science*, 215:1498–1501, 1982.

[42] Y. C. Sud, J. Shukla, and Y. Mintz. Influence of land surface roughness on atmospheric circulation and precipitation: A sensitivity study with a general circulation model. *Journal of Applied Meteorology*, 27:1036–1054, 1988.

[43] J. M. Thornley. A model to describe the partitioning of photosynthate during vegetative plant growth. *Ann. Bot.*, 33:419–430, 1969.

[44] J.M. Thornley. A balanced quantitative model for root,shoot ratios in vegetative plants. *Ann. Bot.*, 36:431–441, 1972.

[45] S. M. Uppala, P. W. Kållberg, A. J. Simmons, U. Andrae, V. da Costa Bechtold, M. Fiorino, J. K. Gibson, J. Haseler, A. Hernandez, G. A. Kelly, X. Li, K. Onogi, S. Saarinen, N. Sokka, R. P. Allan, E. Andersson, K. Arpe, M. A. Balmaseda, A. C. M. Beljaars, L. van de Berg, J. Bidlot, N. Bormann, S. Caires, F. Chevallier, A. Dethof, M. Dragosavac, M. Fisher, M. Fuentes, S. Hagemann, E. Hólm, B. J. Hoskins, L. Isaksen, P. A. E. M. Janssen, R. Jenne, A. P. McNally, J. F. Mahfouf, J. J. Morcrette, N. A. Rayner, R. W. Saunders, P. Simon, A. Sterl, K. E. Trenberth, A. Untch, D. Vasiljevic, P. Viterbo, and J. Woollen. The era-40 re-analysis. *Quarterly Journal of the Royal Meteorological Society*, 131:2961–3012, October 2005.

[46] R. H. Waring, J. J. Landsberg, and M. Williams. Net primary production of forests: a constant fraction of gross primary production? *Tree Physiology*, 18:129–134, 1998.

[47] F. I. Woodward. Stomatal numbers are sensitive to increases in co2 from preindustrial levels. *Nature*, 327:617–618, 1987.

[48] N. Zeng, H. Qian, E. Munoz, and R. Iacono. How strong is carbon cycle-climate feedback under global warming? *Geophys. Res. Lett.*, 31:20203–+, October 2004.

[49] J. Zhang and J. Xu. A hybrid macroevolutionary algorithm. *: Advances in Natural Computation*, pages 299–308, 2005.